A hypoplastic macroelement for single vertical piles in sand subject to three-dimensional loading conditions

Zheng Li, Panagiotis Kotronis, Sandra Escoffier, Claudio Tamagnini

A hypoplastic macroelement for single vertical piles in sand subject to three-dimensional loading conditions

Zheng Li[1,2] · Panagiotis Kotronis[1] · Sandra Escoffier[2] · Claudio Tamagnini[3]

Abstract This paper presents a novel macroelement for single vertical piles in sand developed within the hypoplasticity theory, where the incremental nonlinear constitutive equations are defined in terms of generalized forces, displacements and rotations. Inspired from the macroelement for shallow foundations of Salciarini and Tamagnini (Acta Geotech, 4(3):163–176, 2009), the new element adopts the "intergranular displacement" mutuated from Niemunis and Herle (Mech Cohes Frict Mater, 2:279–299, 1997) to reproduce the behavior under cyclic loading. Analytical and numerical strategies are provided to calibrate the macroelement's parameters. Comparisons with experimental results show the performance of the macroelement that while being simple and computational fast is suitable for finite element calculations and engineering design.

✉ Panagiotis Kotronis
Panagiotis.Kotronis@ec-nantes.fr

Zheng Li
zheng.li@ec-nantes.fr

Sandra Escoffier
sandra.escoffier@ifsttar.fr

Claudio Tamagnini
claudio.tamagnini@unipg.it

[1] LUNAM Université, Ecole Centrale de Nantes, Université de Nantes, CNRS UMR 6183, GeM (Institut de Recherche en Génie Civil et Mécanique), 1 rue de la Noë, BP 92101, 44321 Nantes, France

[2] IFSTTAR, GERS, SV, LUNAM Université, 44341 Bouguenais, France

[3] Department of Civil and Environmental Engineering, Università degli Studi di Perugia, Perugia, Italy

Keywords Foundation · Hypoplasticity · Macroelement · Pile · Soil-structure interaction

1 Introduction

According to the scale adopted for the formulation of the underlying theoretical model, numerical simulations of geotechnical problems can be—and often are—classified in two broad categories: meso-scale and macro-scale computations. In a typical meso-scale approach such as, for example, in the Discrete Element Method (DEM) [7, 13], the description of soil behavior is made at the particle scale. Particles are modeled as rigid bodies, and grain to grain interactions at the contacts are described by means of suitable contact laws. Various successful applications of the DEM method in geotechnical engineering can be found in the literature, see e.g., [6, 19, 71].

In computational geomechanics, the paradigm for the macro-scale approach is provided by the finite element method (FEM), in which a mathematical problem cast within the framework of continuum mechanics is transformed into a discrete algebraic problem by approximating the unknown fields with simple functions with local support, see e.g., [43, 60, 81]. In this case, the description of soil behavior is made at the macroscopic (phenomenological) level, in terms of a suitable constitutive equation providing the stress evolution for a given strain history. The constitutive equation is often formulated in rate-form, in order to capture the non-linear, irreversible and history-dependent character of soil behavior, see, e.g., [16, 75].

In relatively recent times, a new class of macroscopic models have been developed mainly for soil-foundation-structure interaction (SFSI) applications, which can be

considered an "upscaled" version of classical macroscopic models considering the soil as a continuous (albeit, sometimes multiphase) medium. In this approach, called *macroelement modeling*, the global behavior of the foundation and of the soil volume interacting with it is "lumped" into a single, integral, constitutive equation linking the evolution of the resultant loads/moments on the foundation to the corresponding displacements/rotations histories. The macroelement concept was introduced in foundation engineering by Nova and Montrasio [58]; however, it shares some similarities with simplified methods developed in structural engineering, to model, e.g., plastic hinge areas in beam-column joints [17, 20, 62, 69]. As compared to macroscopic approaches based on continuum mechanics, the striking advantages of the macroelement approach are in its remarkable computational efficiency, in the relatively simple formulation of their constitutive equations, and in the ease of numerical implementation into general purpose FE codes.

For the following reasons, this approach has found widespread applications in the modeling of structures with isolated *shallow foundations*. Among the available nonlinear macroelement models of this class present in the literature, we can distinguish two groups, based on the mathematical framework used to construct the constitutive equations:

(a) *Plasticity theory*-based macroelements;
(b) *Hypoplasticity theory*-based macroelements.

In the first group of models, the basic principles of isotropic or anisotropic hardening plasticity are used to define the elastic behavior, the flow rule and the hardening law of the macroelement. All the relevant constitutive functions—i.e., elastic constitutive equation, yield function, plastic potential and hardening laws—are formulated in terms of the (generalized) load vector acting on the foundation and the internal variables accounting for the effects of previous loading history. As in classical plasticity, the standard Prager's consistency condition provides the full set of evolution equations for the soil-foundation system.

As already mentioned, Nova and Montrasio [58] pioneered the development of elastoplastic macroelements for shallow footings, considering a perfectly rigid strip footing resting on a purely frictional soil. Further developments of the macroelement approach for shallow footings under monotonic loading conditions can be found, e.g., in [8, 33, 42, 46, 53]. More recently, the attention has been focused on the simulation of the cyclic/dynamic response of shallow footings for seismic SFSI analysis. Paolucci [59] adopted an elastic-perfectly plastic macroelement with a non-associated flow rule for seismic SFSI simulations. Crémer et al. [11, 12] developed a isotropic/kinematic hardening macroelement for cyclic/dynamic loading conditions incorporating the effects of geometric nonlinearity (foundation uplift), and applied it for cyclic and seismic loading conditions. Grange et al. [34] used a multi-mechanism, isotropic/kinematic hardening model to improve the description of the foundation overturning mechanism and uplift. The same authors successfully combined the macroelement with multifiber Timoshenko beams [41, 47] to evaluate the effects of soil-structure interactions under seismic loadings [35, 36]. Further contributions in this field can be found in [9, 23, 25, 27, 70].

An inelastic, rate-type macroelement model based on the principles of the theory of hypoplasticity [40, 55, 76] has been first developed by Salciarini and Tamagnini [68]. This model, which shares some key features with the elastoplastic macroelement of Nova and Montrasio, differs from the other elastoplastic macroelements mentioned before in the incrementally non-linear character of the constitutive equations, which precludes the existence of an elastic domain in the generalized loading space. The model incorporates a vector-like internal variable (the *internal displacement*) which, accounting for the effects of recent deformation history, allows to reproduce satisfactorily most of the relevant features of the experimentally observed response of the foundation-soil system under rather complex loading paths, including load reversals. Extended versions of the original hypoplastic model have been presented in [66, 67]. A comparison between the predictions provided by the advanced elastoplastic macroelement of Grange et al. [34] and the hypoplastic macroelement of Salciarini and Tamagnini [68] in the seismic SFSI analysis of a 4-span r.c. bridge has been presented in [65].

A third possible approach to macroscopic modeling of shallow footing/soil systems which is somewhat in between the continuum-based finite element (FE) modeling and the use of plasticity- or hypoplasticity-based macroelement models is provided by the so-called "Beam on Non-linear Winkler Foundation" (BNWF) models-based on the work of Bartlett [3] and Wiessing [79] for rocking-dominated strip footings-in which the foundation soil is treated as a (non-linear and possibly unilateral) Winkler bed, sometimes endowed with viscous damping. Recent works in this field include, e.g., Refs. [26, 38, 72, 80].

Although BNWF models for shallow footings appear to have gained some popularity mainly in the structural earthquake engineering community, their main drawback stems from the impossibility of modeling correctly the experimentally observed coupling between the different degrees of freedom of the footing, except, perhaps in rocking-dominated loading conditions. As compared to inelastic macroelements, this drawback of BNWF models is not compensated by their computational efficiency or

ease of implementation. This can explain the relatively large diffusion of macroelement approaches for SFSI analysis of isolated shallow footings.

When the deformation and failure behavior of deep, piled foundations under cyclic/dynamic loading condition is of concern, the current state of the art in SFSI modeling is almost reversed, with BNWF models largely dominating among macroscopic "global" modeling approaches. Notable works in this respect are those of Nogami et al. [57], who combined springs and dashpots to describe soil damping, and of Boulanger et al. [4], who analyzed the seismic soil-pile-structure interaction of a single pile in a two-layer soil, and validated their approach by means of small-scale dynamic model tests in the centrifuge. Subsequent developments include the works of Taciroglu et al. [63, 73], who incorporated frictional forces and gap opening at the pile-soil interface; Curras et al. [14], who extended the BNWF approach to pile group systems; Gerolymos and Gazetas [30–32], who applied the BNWF approach to rigid caissons under static and dynamic loads, and Varun [77], who proposed the use of multiple $p-y$ curves to take into account the effects of pore pressure build-up and liquefaction.

This state of affairs is certainly due to the difficulties encountered in properly defining a complete failure domain for deep foundations, even in the simple case of a single pile, and perhaps to the appeal that BNWF models have for the structural engineer, as they provide important informations concerning the distribution of shear forces and bending moments along the pile axis. However, the same limitations stressed for BNWF shallow footing models apply, perhaps even to a larger extent, to pile models developed within the same approach. In fact, BNWF models require as input data a series of soil pressure–displacement ($p-y$) curves, which are very difficult to select in the absence of data from instrumented lateral pile load tests. For example, Murchison and O'Neill [54], in a study comparing four proposed procedures for selecting $p-y$ curves with data from field tests, have shown that errors in pile-head deflection predictions could be as large as 75 %. It is also uncertain how the $p-y$ curves are affected by pile head constraints and the relative stiffness of the pile and the soil.

One of the first attempts to develop a global non-linear model for a single pile, considering the soil interacting with the pile as a continuous medium, can be found in the works of Davies and Budhu [5, 18], who employed a variable module elastic constitutive equations and modeled the pile-soil interaction using Mindlin solution as in Ref. [2]. A more recent application of the same approach has been presented in [61]. Although more appealing than BNWF models, these approaches still fail to capture the coupling existing between the different degrees of freedom in the nonlinear range.

It is only very recently that, due to the development in both experimental techniques and computing facilities, the problem of developing a single, global constitutive equation capable of reproducing the observed non-linear, irreversible, hysteretic behavior of the soil-pile system under cyclic/dynamic loading conditions has been addressed within the framework of elastoplastic macroelement models, where plastic flow mechanisms are inherently coupled. In particular, Correia [10] introduced an elastoplastic macroelement for a single concrete pile in purely cohesive soil. In his model, coupling is considered only in the horizontal force-bending moment plane, but does not include the effects of the vertical load.

In this paper, a new macroelement for a single pile embedded in a homogeneous sand layer and head located at the ground surface, is developed within the framework of hypoplasticity, inspired from the work of Salciarini and Tamagnini [68] on shallow foundations. The behavior of the pile is assumed linear elastic (no plastic deformations in the pile are considered). The constitutive equations in rate form are defined in terms of generalized forces, displacements and rotations, and are constructed based on the 3D failure envelope for a single pile in Fontainebleau sand (NE34) proposed by Li et al. [45]. The capability of reproducing the non-linear soil-pile response under cyclic loading has been incorporated by introducing a displacement-like internal variable—the *internal displacement* vector—mutuated from the concept of "intergranular strain", first introduced by Niemunis and Herle [56] in the context of continuum hypoplasticity.

The outline of the paper is as follows. In Sect. 2 the details of the mathematical formulation of the model and the numerical strategy adopted for its FE implementation are presented. Section 3 addresses the very important point of macroelement calibration, providing different possible strategies to determine the relevant model constants controlling the model response. In Sect. 4 the performance of the macroelement is assessed by comparing its predictions with available experimental observations from a number of small-scale tests performed under artificial gravity [64]. Section 5 provides some insights concerning the applicability of the proposed macroelement model to more complex stratigraphic conditions. Finally, some concluding remarks and suggestions for further developments are provided in Sect. 6.

In the following, vectors and matrices are represented with boldface symbols. The operator $||\boldsymbol{v}||$ applied to a vector $\boldsymbol{v}$ denotes the Euclidean norm of $\boldsymbol{v}$. The symbol $\boldsymbol{m}^T$ indicates the transpose of a vector/matrix $\boldsymbol{m}$. A superposed dot, like in $\dot{x}$, denotes the time derivative of the variable x.

2 Constitutive equations of the hypoplastic macroelement

2.1 Basic structure of the hypoplastic constitutive equations

In developing the constitutive equation for the pile-foundation system, we assume that the pile head is subjected to a three-dimensional loading system, composed by a vertical, axial load V, an horizontal, tangential load H, and a bending moment M orthogonal to the direction of the horizontal load, so that the deformations of the pile axis are contained in the vertical plane containing the forces V and H. Although such a loading system is not the most general possible, it includes the majority of the cases of practical interest.

In a global macroscopic setting, the mechanical response of the pile-foundation system is described by means of a single constitutive equation between the generalized load vector $\boldsymbol{t}$ and the (work-conjugate) generalized displacement vector $\boldsymbol{u}$, defined as:

$$\boldsymbol{t} := \{V, H, M/d\}^{\mathrm{T}} \qquad \boldsymbol{u} := \{w, u, d\theta\}^{\mathrm{T}} \tag{1}$$

where w, u and θ are the pile head vertical displacement, horizontal displacement and rotations, respectively, and d is the pile diameter, used here as a characteristic length scale to homogeneize the dimensions of the components of $\boldsymbol{t}$ and $\boldsymbol{u}$.

According to [68], the basic structure of the constitutive equation in rate-form for a hypoplastic macroelement, in the simplest possible case in which the state of the system is sufficiently represented by the current load $\boldsymbol{t}$, is given by:

$$\dot{\boldsymbol{t}} = \boldsymbol{\mathcal{L}}(\boldsymbol{t})\dot{\boldsymbol{u}} + \boldsymbol{N}(\boldsymbol{t})||\dot{\boldsymbol{u}}|| \tag{2}$$

where the matrix $\boldsymbol{\mathcal{L}}$ and the vector $\boldsymbol{N}$ are suitable constitutive functions to be defined based on available experimental evidence on the system response. In Eq. (2), the first term on the right-hand side represents the *incrementally linear* part of the constitutive equation. The second term, nonlinear in $\dot{\boldsymbol{u}}$, is responsible for the *incremental non-linearity* of the system response, i.e., for the continuous dependence of the system stiffness on the loading direction, see, e.g., [15, 76]. This feature of the hypoplastic constitutive Eq. (2) can be better appreciated by recasting it in the following quasi-linear format:

$$\dot{\boldsymbol{t}} = \boldsymbol{\mathcal{K}}(\boldsymbol{t}, \boldsymbol{\eta})\, \dot{\boldsymbol{u}} \tag{3}$$

in which the *tangent stiffness matrix* $\boldsymbol{\mathcal{K}}$ is given by:

$$\boldsymbol{\mathcal{K}} = \boldsymbol{\mathcal{L}}(\boldsymbol{t}) + \boldsymbol{N}(\boldsymbol{t})\boldsymbol{\eta}^T \quad \boldsymbol{\eta} := \frac{\dot{\boldsymbol{u}}}{||\dot{\boldsymbol{u}}||} \tag{4}$$

Looking at Eq. $(4)_1$, it is immediately apparent that the tangent stiffness matrix varies continuously with the direction $\boldsymbol{\eta}$ of the system generalized velocity $\dot{\boldsymbol{u}}$. This is a characteristic feature of hypoplasticity which—together with the absence of any decomposition of displacement rates into an elastic and a plastic part—marks a significant difference with elastoplasticity, where the stiffness matrix assumes only two possible values at each state, one for plastic loading and one for elastic unloading.

2.2 Extension to cyclic/dynamic loading conditions

The constitutive Eqs. (2) or (3) is suitable for monotonic loading conditions, but the impossibility of distinguishing loading states characterized by the same value of $\boldsymbol{t}$ but different loading histories makes it unsuitable to reproduce the behavior of the pile-soil system under cyclic/dynamic loading conditions.

In order to do that, the model should be enriched with a set of suitable internal variables capable of taking into account the effects of the previous loading history on the system response. Following Salciarini and Tamagnini [68], this is obtained by introducing a new displacement-like vectoria internal variable, $\boldsymbol{\delta}$, defined *internal displacement*. This internal variable mimics the "intergranular strain" tensor, introduced by Niemunis and Herle [56] in the context of continuum hypoplasticity.

In the enriched version of the hypoplastic macroelement model, the internal displacement vector is defined by the following evolution equation:

$$\dot{\boldsymbol{\delta}} = \widehat{\boldsymbol{\mathcal{H}}}(\boldsymbol{\delta}, \boldsymbol{\eta})\dot{\boldsymbol{u}} \quad \widehat{\boldsymbol{\mathcal{H}}} = \begin{cases} \boldsymbol{\mathcal{I}} - \rho^{\beta_r}\boldsymbol{\eta}_\delta\boldsymbol{\eta}_\delta^T & \text{if } \boldsymbol{\eta}_\delta \cdot \boldsymbol{\eta} > 0; \\ \boldsymbol{\mathcal{I}} & \text{if } \boldsymbol{\eta}_\delta \cdot \boldsymbol{\eta} \leq 0. \end{cases} \tag{5}$$

where $\boldsymbol{\mathcal{I}}$ is the identity matrix, the unit vector $\boldsymbol{\eta}_\delta$ and the scalar ρ define the internal displacement direction and a normalized measure of its magnitude, respectively:

$$\boldsymbol{\eta}_\delta := \begin{cases} \boldsymbol{\delta}/||\boldsymbol{\delta}|| & (\text{if } ||\boldsymbol{\delta}|| > 0) \\ \boldsymbol{0} & (\text{if } ||\boldsymbol{\delta}|| = 0) \end{cases} \qquad \rho := \frac{1}{R}||\boldsymbol{\delta}|| \tag{6}$$

while β_r and R are model constants. In a deformation process starting from a very low (or zero) magnitude of the internal displacement, $\rho \simeq 0$ and $\underline{\boldsymbol{\delta}} \simeq \dot{\boldsymbol{u}}$. If the system continues to move in the same direction (i.e., at constant $\boldsymbol{\eta}$) eventually ρ approaches 1 ($||\boldsymbol{\delta}|| \to R$). At this point, $\boldsymbol{\delta}$ remains constant and $\boldsymbol{\eta}_\delta = \boldsymbol{\eta}$: the internal displacement vector remains constant and aligned with the system trajectory. We expect that in such a state, the response of the system would be identical to the one predicted by the constitutive Eq. (2) of the standard macroelement.

However, if the displacement path of the system experience a complete reversal, the difference between the unit vectors $\boldsymbol{\eta}_\delta$ and $\boldsymbol{\eta} = -\boldsymbol{\eta}_\delta$ registers that the system is undergoing a load reversal process. In such a condition, we expect the response of the system to be quasi-elastic, with a

stiffness higher than in the previous loading stage. The particular formulation of the evolution Eq. (5) guarantees that the transition between this pseudo-elastic behavior and the fully non-linear, asymptotic hypoplastic regime requires some further deformation along the new loading path.

The model constants R and β_r control the magnitude of the additional displacements required to reach the asymptotic hypoplastic regime and the speed at which the realignment between the vectors $\boldsymbol{\eta}_\delta$ and $\boldsymbol{\eta}$ may take place.

Taking into account the previous observations concerning the evolution of the internal displacement during a given loading process, the expected cyclic response of the system can be obtained by modifying the constitutive equations of the macroelement as follows:

$$\dot{\boldsymbol{t}} = \widehat{\boldsymbol{\mathcal{K}}}(\boldsymbol{t}, \boldsymbol{\delta}, \boldsymbol{\eta})\, \dot{\boldsymbol{u}} \tag{7}$$

where:

$$\widehat{\boldsymbol{\mathcal{K}}} = [\rho^\chi m_T + (1-\rho^\chi) m_R]\boldsymbol{\mathcal{L}}(\boldsymbol{t}) + \widetilde{\boldsymbol{\mathcal{K}}}(\boldsymbol{t}, \boldsymbol{\delta}, \boldsymbol{\eta}) \tag{8}$$

$$\widetilde{\boldsymbol{\mathcal{K}}} = \begin{cases} \rho^\chi (1-m_T)(\boldsymbol{\mathcal{L}}\boldsymbol{\eta}_\delta)\boldsymbol{\eta}_\delta^T + \rho^\chi \boldsymbol{N}\boldsymbol{\eta}_\delta^T & (\text{if} \quad \boldsymbol{\eta}_\delta \cdot \boldsymbol{\eta} > 0) \\ \rho^\chi (m_R - m_T)(\boldsymbol{\mathcal{L}}\boldsymbol{\eta}_\delta)\boldsymbol{\eta}_\delta^T & (\text{if} \quad \boldsymbol{\eta}_\delta \cdot \boldsymbol{\eta} \le 0) \end{cases} \tag{9}$$

where χ, m_T and m_R are model constants.

Equations (8) and (9) define a smooth interpolation law for the stiffness matrix of the pile-soil system between the following limiting cases:

(a) *continued loading* at constant $\boldsymbol{\eta}$, with $||\boldsymbol{\delta}|| = R$ and $\boldsymbol{\eta}_\delta = \boldsymbol{\eta}$; in this case, the system is in the full hypoplastic regime, and:

$$\begin{aligned} \dot{\boldsymbol{t}} &= m_T \boldsymbol{\mathcal{L}}\dot{\boldsymbol{u}} + (1-m_T)\boldsymbol{\mathcal{L}}\boldsymbol{\eta}_\delta(\boldsymbol{\eta}_\delta^T \dot{\boldsymbol{u}}) + \boldsymbol{N}\boldsymbol{\eta}_\delta^T \dot{\boldsymbol{u}} \\ &= \boldsymbol{\mathcal{L}}\dot{\boldsymbol{u}} + \boldsymbol{N}||\dot{\boldsymbol{u}}|| \end{aligned} \tag{10}$$

since $(\boldsymbol{\eta}_\delta^T \dot{\boldsymbol{u}})\boldsymbol{\eta}_\delta = (\boldsymbol{\eta}^T \dot{\boldsymbol{u}})\boldsymbol{\eta} = \dot{\boldsymbol{u}}$ and $\boldsymbol{\eta}_\delta^T \dot{\boldsymbol{u}} = \boldsymbol{\eta}^T \dot{\boldsymbol{u}} = ||\dot{\boldsymbol{u}}||$;

(b) *orthogonal loading* with $\boldsymbol{\eta}_\delta^T \boldsymbol{\eta} = 0$ and $||\boldsymbol{\delta}|| = R$; in this case, the response of the system is hypoelastic, as:

$$\dot{\boldsymbol{t}} = m_T \boldsymbol{\mathcal{L}}\dot{\boldsymbol{u}} + (m_R - m_T)\boldsymbol{\mathcal{L}}\boldsymbol{\eta}_\delta(\boldsymbol{\eta}_\delta^T \dot{\boldsymbol{u}}) = m_T \boldsymbol{\mathcal{L}}\dot{\boldsymbol{u}} \tag{11}$$

as $\boldsymbol{\eta}_\delta^T \dot{\boldsymbol{u}} = \boldsymbol{\eta}_\delta^T \boldsymbol{\eta} ||\dot{\boldsymbol{u}}|| = 0$;

(c) *full load reversal* with $\boldsymbol{\eta}_\delta = -\boldsymbol{\eta}$ and $||\boldsymbol{\delta}|| = R$; in this case, the system response is again hypoelastic, as in case (b), but characterized by a different stiffness:

$$\dot{\boldsymbol{t}} = m_T \boldsymbol{\mathcal{L}}\dot{\boldsymbol{u}} + (m_R - m_T)\boldsymbol{\mathcal{L}}\boldsymbol{\eta}_\delta(\boldsymbol{\eta}_\delta^T \dot{\boldsymbol{u}}) = m_R \boldsymbol{\mathcal{L}}\dot{\boldsymbol{u}} \tag{12}$$

as $(\boldsymbol{\eta}_\delta^T \dot{\boldsymbol{u}})\boldsymbol{\eta}_\delta = (\boldsymbol{\eta}^T \dot{\boldsymbol{u}})\boldsymbol{\eta} = \dot{\boldsymbol{u}}$.

Equations (10)–(12) provide also the physical interpretation of the role played by the model constants m_T, m_R and χ. The first two affect the magnitude of the apparent hypoelastic stiffness matrix for orthogonal and full reverse loading, respectively. Typically, $m_R > m_T$ as the response under full loading reversal is generally stiffer than under orthogonal loading. The third constant χ controls the speed at which the three limiting cases are reached as ρ approaches 1.

In order to complete the description of the hypoplastic macroelement constitutive equations, it is necessary to define the constitutive functions $\boldsymbol{\mathcal{L}}$ and $\boldsymbol{N}$. This point is addressed in the following sections.

2.3 Constitutive matrix $\boldsymbol{\mathcal{L}}$

Considering that for a full load reversal the incremental response of the system can be described by a (pseudo) elastic stiffness matrix $\boldsymbol{\mathcal{K}}^e$ and taking into account Eq. (12), we can link the constitutive matrix $\boldsymbol{\mathcal{L}}$ to the stiffness matrix $\boldsymbol{\mathcal{K}}^e$ by means of the following simple relation:

$$\boldsymbol{\mathcal{K}}^e = m_R \boldsymbol{\mathcal{L}} \quad \Leftrightarrow \quad \boldsymbol{\mathcal{L}} = \frac{1}{m_R}\boldsymbol{\mathcal{K}}^e = \frac{1}{m_R}\begin{bmatrix} k_{vv} & 0 & 0 \\ 0 & k_{hh} & k_{hm} \\ 0 & k_{hm} & k_{mm} \end{bmatrix} \tag{13}$$

where k_{vv}, k_{hh}, k_{mm} and k_{hm} are the vertical, horizontal, rotational and coupled horizontal-rotational stiffness coefficients of the pile-soil system, obtained, e.g., from fundamental solutions of the theory of elasticity. In this case, differently from what is typically observed in the response of shallow footings—see, e.g., [34]—the coupling coefficent k_{hm} is not negligible as compared to the direct stiffness coefficients k_{vv}, k_{mm}.

2.4 Constitutive vector $\boldsymbol{N}$

Since the nonlinear part of the constitutive Eq. (2) or (7)—controls the response of the system near or at failure states, the definition of a failure locus in the generalized stress state is a fundamental step towards its definition. In this work, we adopt the failure surface proposed by Li et al. [45] for a single pile in sand (Fontainebleau sand NE34), defined by the following failure criterion:

$$\begin{aligned} F(\boldsymbol{t}) = &\left(\frac{H}{H_0}\right)^2 + \left(\frac{M}{M_0}\right)^2 - \alpha\left(\frac{H}{H_0}\right)\left(\frac{M}{M_0}\right) \\ &- 1 + \left\{\mathcal{H}(V)\left(\frac{V_{t0}}{V_{c0}}\right)^2 + \mathcal{H}(-V)\right\}\left(\frac{V}{V_{t0}}\right)^2 = 0 \end{aligned} \tag{14}$$

The failure surface described by Eq. (14) is shown in Fig. 1 in the three-dimensional loading space. In Eq. (14), the constants H_0, M_0, V_{c0} and V_{t0} represent the failure loads under pure horizontal, bending, axial compression and axial tension loads, respectively, while the coupling

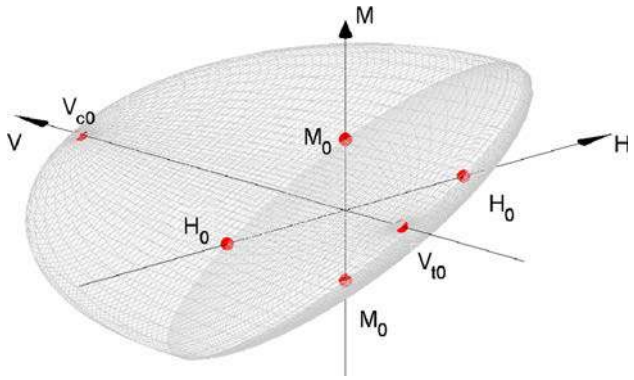

Fig. 1 Three-dimensional failure surface proposed by Li et al. [45], plotted for V_{t0} = 5100 kN; V_{c0} = 25000 kN; H_0 = 5000 kN; M_0 = 0.42 $\times 10^5$ kNm, and α = 1.5

constant α controls the orientation of the failure surface in the $H : M/d$ plane. The symbol $\mathcal{H}(x)$ denotes the Heaviside step function, defined by:

$$\mathcal{H}(x) = \begin{cases} 1 & \text{if} \quad x > 0 \\ 0 & \text{if} \quad x \leq 0 \end{cases}$$

Its use in the two terms within curly brackets in Eq. (14) allows to switch from failure under axial compression states ($V > 0$) to failure under axial tension states ($V \leq 0$).

As shown in [55], the failure locus defined by Eq. (14) can be incorporated in the hypoplastic model by defining the constitutive function $\boldsymbol{N}$ as follows:

$$\boldsymbol{N}(\boldsymbol{t}) = -Y(\boldsymbol{t})\boldsymbol{\mathcal{L}}\,\boldsymbol{m}(\boldsymbol{t}) \tag{15}$$

where $\boldsymbol{m}$ is a unit vector oriented in the opposite direction of $L^{-1}N$, and the scalar function $Y(\boldsymbol{t}) \in [0, 1]$—called *loading function*—is defined so that: (1) it is equal to 1 for loading states on the failure surface; and, (2) it decreases monotonically with increasing distance from the failure surface. With this definition, in fully hypoplastic loading states the constitutive equation of the macroelement reads:

$$\dot{\boldsymbol{t}} = \boldsymbol{\mathcal{L}}\,\{\dot{\boldsymbol{u}} - Y(\boldsymbol{t})\boldsymbol{m}\,||\dot{\boldsymbol{u}}||\} \tag{16}$$

It is clear from Eq. (16) that the loading function Y quantifies the degree of nonlinearity in the model response. In the limit $Y \to 0$, the response of the macroelement becomes hypoelastic. When the pile-soil system reaches failure, $\dot{\boldsymbol{t}} = \boldsymbol{0}$ and $Y = 1$. From Eq. (16) we obtain:

$$\boldsymbol{m} = \left(\frac{\dot{\boldsymbol{u}}}{||\dot{\boldsymbol{u}}||}\right)_f = \boldsymbol{\eta}_f \tag{17}$$

The unit vector $\boldsymbol{m}$ thus provides the direction of the macroelement velocity at failure (plastic flow direction). Assuming for simplicity an associative plastic flow rule in the generalized loading space, we can evaluate the vector $\boldsymbol{m}$ for states on the failure surface as follows:

$$\boldsymbol{m}_f = \frac{1}{\left|\left|\dfrac{\partial F}{\partial \boldsymbol{t}}\right|\right|}\frac{\partial F}{\partial \boldsymbol{t}} \tag{18}$$

The loading function Y is defined by assuming that for each loading state $\boldsymbol{t}$ inside the failure surface, an image state $\boldsymbol{t}^*$ is defined on the failure surface by a simple projection from the origin of the loading space:

$$\boldsymbol{t}^* = \frac{1}{\xi}\,\boldsymbol{t} \qquad \xi \in (0, 1] \tag{19}$$

The value of ξ can be computed imposing the condition $f(\boldsymbol{t}^*) = 0$, which yields the following simple solution:

$$\xi = \sqrt{\left(\frac{H}{H_0}\right)^2 + \left(\frac{M}{M_0}\right)^2 - \alpha\left(\frac{H}{H_0}\right)\left(\frac{M}{M_0}\right) + \left(\frac{V}{V_0}\right)^2} \tag{20}$$

where $V_0 = V_{c0}$ for $V > 0$ and $V_0 = V_{t0}$ otherwise.

Taking ξ as a suitable measure of the distance of the current loading state from the failure surface, we adopt the following simple power law for the loading function Y:

$$Y(\boldsymbol{t}) = \xi^{\kappa} \tag{21}$$

with κ a material constant controlling the stiffness decay of the model response upon monotonic loading paths at constant $\boldsymbol{\eta}$.

From a purely geometric point of view, the condition $f(\xi\boldsymbol{t}) = 0$ can be interpreted as the definition of a *loading surface*, homothetic to the failure surface $F(\boldsymbol{t}) = 0$, but of smaller size:

$$f(\boldsymbol{t}) = \left(\frac{H}{h_0}\right)^2 + \left(\frac{M}{m_0}\right)^2 - \alpha\left(\frac{H}{h_0}\right)\left(\frac{M}{m_0}\right) - 1 + \left\{\mathcal{H}(V)\left(\frac{v_{t0}}{v_{c0}}\right)^2 + \mathcal{H}(-V)\right\}\left(\frac{V}{v_{t0}}\right)^2 = 0 \tag{22}$$

with:

$$\begin{aligned} v_{c0} &= \xi\, V_{c0} \leq V_{c0} \quad v_{t0} = \xi\, V_{t0} \leq V_{t0} \\ h_0 &= \xi\, H_0 \leq H_0 \quad m_0 = \xi\, M_0 \leq M_0 \end{aligned} \tag{23}$$

A representation of the loading and failure surfaces in the three-dimensional loading space is given in Fig. 2.This geometrical interpretation suggests that, for all the admissible loading states, the vector $\boldsymbol{m}$ can be defined as the unit gradient to the loading surface:

$$\boldsymbol{m} = \frac{1}{\left|\left|\dfrac{\partial f}{\partial \boldsymbol{t}}\right|\right|}\frac{\partial f}{\partial \boldsymbol{t}} \tag{24}$$

Obviously, when $\xi = 1$ the functions F and f coincide and Eq. (24) provides the same result as Eq. (18).

The failure condition provided by Eq. (14) represents an attractor for the evolution Eq. (16), so that for proportional

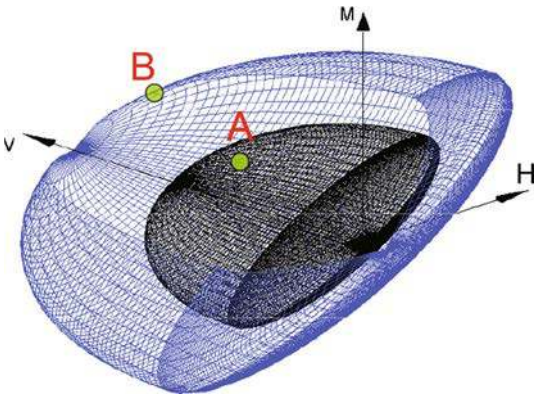

Fig. 2 Loading and failure surfaces in the generalized loading space. In the figure, a is the current loading state and b its image state on the failure surface

displacement paths the generalized load $\boldsymbol{t}$ will converge toward it. However, this does not guarantee that, for complex loading conditions, the loading path will never cross it, reaching states with $f > 0$ (or $Y > 1$). In order to overcome this problem, the following modification has been introduced to the flow direction vector $\boldsymbol{m}$ in the vicinity of the failure surface:

$$\boldsymbol{m} = \frac{\boldsymbol{v}}{||\boldsymbol{v}||} \qquad \boldsymbol{v} = [1 - \mathcal{H}_s(Y, \epsilon)]\, \boldsymbol{m}_f + \mathcal{H}_s(Y, \epsilon)\, \boldsymbol{\eta} \tag{25}$$

where $\boldsymbol{\eta}$ is the generalized velocity direction, $\boldsymbol{m}_f$ is provided by Eq. (18) and $\mathcal{H}_s$ is a smoothed Heaviside step function defined as:

$$\mathcal{H}_s(Y, \epsilon) = \begin{cases} 0 & \text{for } Y \leq 1 \\ \dfrac{1}{2}\left[1 - \cos\left(\dfrac{Y-1}{\epsilon}\,\pi\right)\right] & \text{for } 1 < Y \leq 1 + \epsilon \\ 1 & \text{for } Y > 1 + \epsilon \end{cases} \tag{26}$$

with ϵ a small regularizing coefficient. According to Eq. (27), the flow direction $\boldsymbol{m}$ equals $\boldsymbol{m}_f$ on the failure surface, while for states characterized by $Y \geq 1 + \epsilon$, $\boldsymbol{m}$ is set equal to $\boldsymbol{\eta}$, thus forcing $\dot{\boldsymbol{t}} \simeq \boldsymbol{0}$ according to Eq. (16). A linear interpolation between these two limits is adopted in the region where $Y \in (1, 1 + \epsilon)$. A series of preliminary numerical simulations has shown that a value of $\epsilon = 10^{-6}$ can be considered adequate in most circumstances.

2.5 Numerical implementation issues

The practical application of the hypoplastic macroelement in the analysis of SFSI problems requires its implementation in a FE code as a user-defined element. In particular, a fundamental task that the element routine has to address is the numerical integration of the constitutive equations Eqs. (5) and (8), for a given displacement history, in order to compute the internal force vector at each global equilibrium iteration.

In this work, the integration algorithm adopted is the explicit, embedded Runge–Kutta scheme of the 3rd order with adaptive substepping and error control proposed in [74] for a hypoplastic macroelement for shallow footings. Let $[t_n, t_{n+1}]$ be the time interval corresponding to a generic time step, and let $\Delta\boldsymbol{u}_{n+1}$ be the prescribed displacement increment obtained from the solution of the global equilibrium equations at a given iteration. Due to the rate-independent character of the constitutive equations, the evolution problem provided by Eqs. (5) and (8) can be recast in terms of the following non-dimensional time measure:

$$T = \frac{t - t_n}{t_{n+1} - t_n} = \frac{t - t_n}{\Delta t_{n+1}} \qquad \text{so that : } \frac{\mathrm{d}}{\mathrm{d}t}(\cdot) = \frac{1}{\Delta t_{n+1}} \frac{\mathrm{d}}{\mathrm{d}T}(\cdot)$$

As the velocity $\dot{\boldsymbol{u}}$ is assumed constant during the time step, the constitutive equations of the macroelement define the following standard system of ODEs:

$$\begin{aligned} &\frac{\mathrm{d}\boldsymbol{x}}{\mathrm{dT}} = \boldsymbol{F}(\boldsymbol{x}) \qquad \text{where} \qquad \boldsymbol{x} := \begin{Bmatrix} \boldsymbol{t} \\ \boldsymbol{\delta} \end{Bmatrix} \\ &\qquad \text{and} \qquad \boldsymbol{F} := \begin{Bmatrix} \widehat{\mathcal{K}} \Delta\boldsymbol{u}_{n+1} \\ \widehat{\mathcal{H}} \Delta\boldsymbol{u}_{n+1} \end{Bmatrix} \end{aligned} \tag{27}$$

The integration of Eq. $(27)_1$ is performed using an adaptive substepping strategy in which the normalized time step [0, 1] is split into substeps $\Delta T_{k+1} = T_{k+1} - T_k$ such that $\sum \Delta T_k = 1$. Let $\tilde{\boldsymbol{x}}_{k+1}$ and $\hat{\boldsymbol{x}}_{k+1}$ be the solution at time T_{k+1} provided by 2nd- and 3rd-order explicit Runge–Kutta schemes, respectively, and let:

$$R_{k+1} := \frac{||\boldsymbol{R}_{k+1}||}{||\hat{\boldsymbol{x}}_{k+1}||} \qquad \text{with:} \qquad \boldsymbol{R}_{k+1} := \hat{\boldsymbol{x}}_{k+1} - \tilde{\boldsymbol{x}}_{k+1}$$

be a measure of the relative difference between the two solutions. For a prescribed error tolerance TOL, the solutions obtained meet the required accuracy level if $R_{k+1} < \mathrm{TOL}$. Thus, $\boldsymbol{x}_{k+1} = \hat{\boldsymbol{x}}_{k+1}$ and the integration procedure continues with a new substep. A new, larger substep size is computed according to the following extrapolation formula:

$$\Delta T_{k+2} = \min\left\{ 0.9\, \Delta T_{k+1} \left(\frac{\mathrm{TOL}}{R_{k+1}}\right)^{1/3};\quad 4\, \Delta T_{k+1};\ 1 - T_k \right\} \tag{28}$$

If, on the contrary, $R_{k+1} \geq \mathrm{TOL}$ the substep is rejected and a new, smaller substep size is computed according to the following extrapolation formula:

$$\Delta T_{k+1} \quad \max\left\{0.9\,\Delta T_{k+1}\left(\frac{\mathrm{TOL}}{R_{k+1}}\right)^{1/3};\ \frac{1}{4}\,\Delta T_{k+1}\right\} \qquad (29)$$

From Eqs. (28) and (29), it is apparent that the extrapolation to bigger substep sizes after an accepted substep is limited to four times the initial value (or by the time increment necessary to reach the final time station $T = 1$), while the reduction of substep size after a rejected substep is limited to 25 % of the initial value.

The integration algorithm has been implemented in the finite element Matlab toolbox FedeasLab [24], developed at the University of California, Berkeley. This FE platform has been used in all the simulations presented in the following Sects. 3, 4 and 5.

3 Calibration of macroelement constants

The hypoplastic macroelememt for a single pile is fully characterized by the pile diameter d and 15 model constants, collected in 4 groups as shown in Table 1. The first group collects the four stiffness coefficients defining the pseudo-elastic response of the system upon load reversal, Equation (13); the second group is composed by the 5 constants entering in the definition of the failure surface, Eq. (14); the third group is made by the loading function constant κ only, Eq. (21); and, finally, the fourth group collects all the constants controlling the response of the model under cyclic loading conditions, Eqs. (5)–(9).

In the following, we describe the calibration procedures adopted for the particular problem of the single pile in sand considered in the small-scale model tests performed by Rosquoët [64] under artificial gravity at the centrifuge facility of IFSTTAR Nantes. The pile geometry is illustrated in Fig. 3. At the prototype scale, the tested pile has an embedded length L = 13 m; a diameter d = 0.72 m; a stiffness $E_p = 3.8\times10^4$ MPa, and a bending stiffness $E_pI_p = 2638 \times 10^6$ Nm^2. The soil in which the pile is immersed is a homogeneous dry Fontainebleau sand (NE34) layer, with a unit weight γ = 16.30 kN/m^3 and a relative density D_r = 86 %.

Two different calibration strategies have been considered:

(a) calibration based on 3d FE simulations and experimental results from Rosquoët [64] cyclic loading tests (Sect. 3.1); and
(b) calibration based on empirical correlations (Sect. 3.2).

In both cases, the performance of the macroelement is validated using experimental results obtained in a new series of centrifuge tests (see Sect. 4).

Table 1 Summary of hypoplastic macroelement constants

Constant	Description	Group
k_{vv}	Vertical stiffness	Pseudo-elastic stiffness
k_{hh}	Horizontal stiffness	
k_{mm}	Rotational stiffness	
k_{hm}	Coupled translation-rotation stiffness	
H_0	Limit horizontal load	Failure surface
M_0	Limit bending moment	
V_{c0}	Axial bearing capacity (compr.)	
V_{t0}	Axial bearing capacity (tens.)	
α	*H vs.* (M/d) coupling coefficient	
κ	Loading function constant	Stiffness degradation
m_R	Stiffness at load reversal point	Cyclic behavior (internal displacement)
m_T	Stiffness when neutral loading	
R	Range of linearity	
β^r	Rate of evolution of IS	
χ	Transition of stiffness	

3.1 Calibration based on 3d FE simulations and experimental results

In this approach, the results of a series of 3d FE simulations of the soil-pile behavior is used to obtain information on the different macroelement constants. Figure 4 shows the FE model adopted in the simulations of Rosquoët tests. The load on the pile head is applied in the X direction. Thus, the Z = const. plane containing the pile axis is a plane of symmetry. The bottom of the soil layer is modeled as a rigid, perfectly rough plane ($\boldsymbol{u}$ = 0). Zero normal displacements and tangential tractions have been imposed on the remaining (fictitious) lateral boundaries of the soil volume.

In the simulations, two different constitutive models have been used for the soil: a linear elastic, isotropic model with (small-strain) shear modulus G_0 varying with depth according to Hardin's empirical equation [39], and the hypoplastic model for sand proposed by von Wolffersdorff [78], in the cyclic loading version with intergranular strain proposed in [56]. The Abaqus implementation of von Wolffersdorff model freely available in the *Soilmodels Project* website [37] has been used in this work. The elastic model has been used to characterize the pseudo-elastic response of the macroelement upon unloading, while the fully inelastic hypoplastic model has been used to characterize the failure locus of the pile-soil system and the stiffness degradation properties of the model.

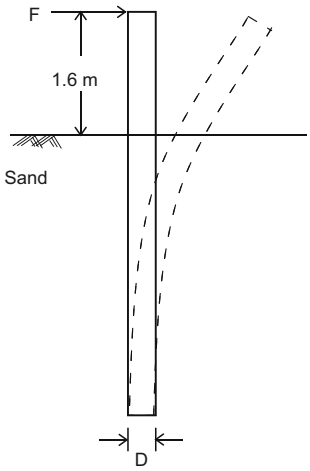

Fig. 3 Geometric layout of cyclic loading tests on a single vertical pile by Rosquoët [64]

Table 2 Material constants of von Wolffersdorff model for Fountainebleau sand

Constant	Description	Value
ϕ	Critical state friction angle (deg.)	31.6
h_s	Granular hardness (MPa)	4800
n	Exponent of limiting void ratio curves (–)	0.29
e_{d0}	Reference minimum void ratio (–)	0.37
e_{c0}	Reference critical void ratio (–)	0.88
e_{i0}	Reference maximum void ratio (–)	0.99
α	Dependency of peak friction (–)	0.24
β	Dependency of soil stiffness (–)	1.97
m_R	Intergranular strain constants (–)	5.0
m_T		2.0
r_{uc}		$1.e^{-4}$
β_r		0.8
χ		6.0

The hypoplastic constitutive model has been calibrated using triaxial test results on Fontainebleau sand from ref. [1]. The values of the material constants thus determined are reported in Table 2, see [44] for the details of the calibration process. A comparison between the experimentally observed behavior of Fountainebleau sand and the hypoplastic model predictions under drained TX compression at different confining pressures is reported in Fig. 5, which shows a very good agreement between predictions and measurements at the local representative elementary volume (REV) level. The comparison between the numerical prediction of the pile head horizontal displacements in a horizontal cyclic loading test—shown in Fig. 6—demonstrates that the good predictive capabilities of the continuum hypoplastic model carry over to the boundary value problem level as well, even for cyclic loading conditions.

The constants V_{c0}, V_{t0}, H_0 and M_0—representing the bearing capacity of the pile for pure vertical (compression and extension), horizontal and bending loads, respectively, and the H:(M/d) coupling coefficient α—have been determined from the extensive program of loading tests conducted by Li et al. [45] with the 3d FE model to investigate the failure condition of the pile-soil system under general three-dimensional loading conditions. The corresponding values are listed in Table 4.

The pseudo-elastic stiffness coefficients have been evaluated from the response of the pile-soil system to the following simple loading conditions:

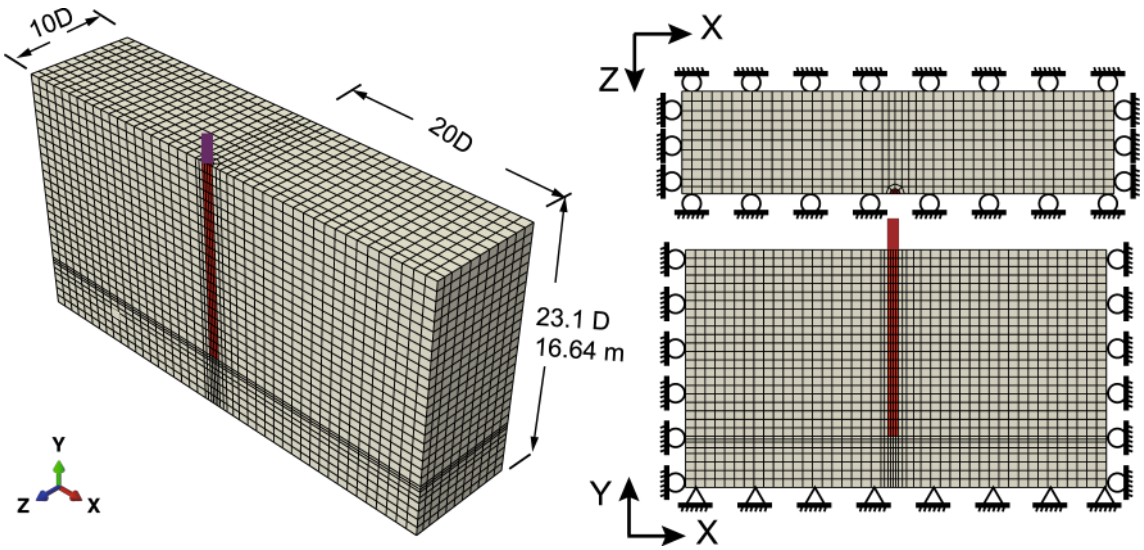

Fig. 4 Finite element model adopted in the macroelement calibration

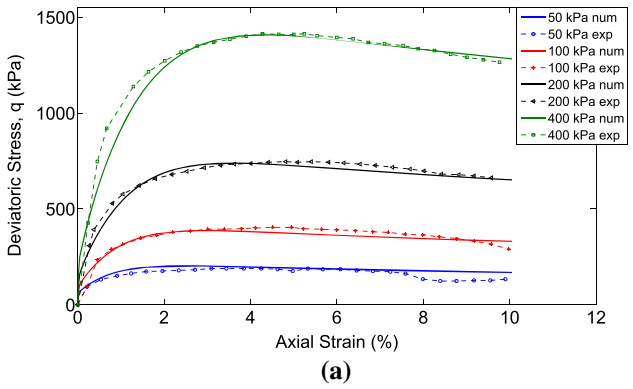

Fig. 5 Comparison of TX-CD test results of Andria–Ntoanina et al. [1] on Fontainebleau sand (NE34) and von Wolffersdorff hypoplastic model predictions, for different confining stresses: **a** deviatoric stress versus axial strain; **b** volumetric strain versus axial strain

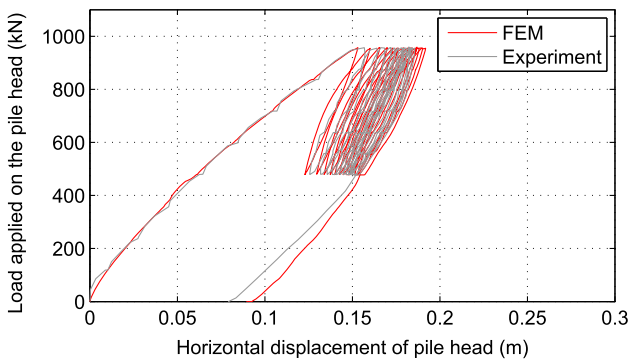

Fig. 6 FEM model with the von Wolffersdorff hypoplastic law and Rosquoët's cyclic tests on a lateral loaded pile [64]

(a) the horizontal k_{hh} and coupling k_{hm} stiffness components are obtained by applying a small horizontal displacement on the pile head while keeping its rotation fixed (Fig. 7a);
(b) the bending k_{mm} and coupling k_{mh} stiffness coefficients are obtained by applying a small rotation on the pile head while keeping the horizontal displacement fixed (Fig. 7b). The quantities k_{hm} and k_{mh} are identical in the pseudo-elastic regime;
(c) the axial stiffness coefficient k_{vv} is obtained by applying a small vertical displacement on the pile-head.

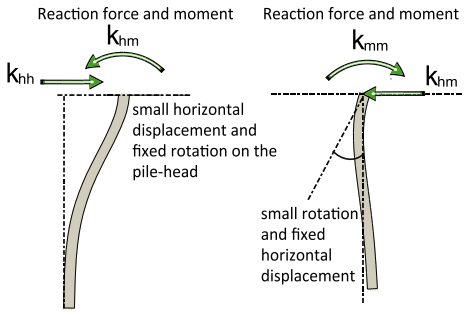

Fig. 7 Loading conditions adopted in the FE model to determine the stiffness coefficients k_{hh}, k_{mm} and k_{hm}

In running these calibration simulations, both the elastic and the von Wolffersdorff models have been adopted for the sand, obtaining substantially identical stiffness constants, as long as the von Wolffersdorff model remains in the pseudo-elastic range within the entire soil mass. The values adopted for the 3 stiffness constants are reported in Table 4.

For the calibration of the loading function constant κ, a single 3d FE simulation of a purely horizontal loading path has been carried out to provide the load-displacement response of the system for a large range of applied displacements ($u_{\max}$ = 1.0 m). The results obtained are shown in Fig. 8, in the H:u plane. The results of a series of macroelement simulations for the same loading path and different values of κ are shown in the same figure. The comparison between the load-displacement curve obtained in the 3d FE simulation and the macroelement prediction indicate an optimum value for κ = 1.2. Note that, for the monotonic character of the loading path and the magnitude of the imposed maximum displacements, the constants m_R, m_T, R, β_r and χ, controlling the cyclic macroelement response, have no effect on the computed results, except for the initial part of the loading path.

The remaining constants, related to the cyclic response of the pile-soil system, have been calibrated by comparing the macroelement predictions directly with the experimental data from a cyclic horizontal loading test provided by Rosquoët [64], using a trial and error procedure to find the optimum set of values. This task is facilitated by the fact that the macroelement response is not so sensitive to the constants β_r and χ. The size R of the pseudo-elastic domain in the generalized displacement space can be guessed from the lenght of the quasi-linear portion of the load-displacement curves upon unloading or reloading,

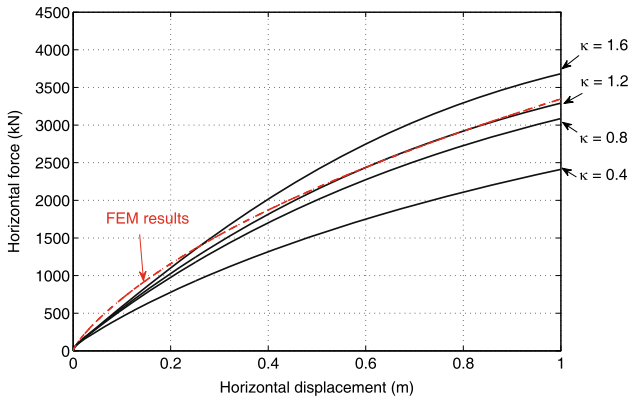

Fig. 8 Comparison between FE prediction of monotonic horizontal loading path (*red dashed curve*) and macroelement response for different values of κ (*solid curves*)

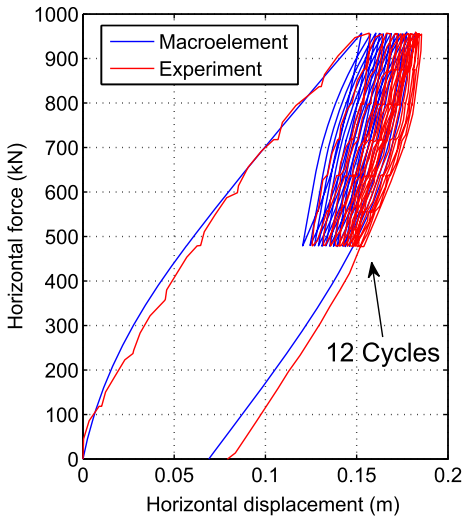

Fig. 9 Comparison between experimental results and macroelement response for cyclic horizontal loading test. Data from Rosquoët [64]

while the constants m_R and m_T affect the ratio between the system stiffness under reverse or tangential loading and continued loading conditions. The values adopted for the 5 cyclic loading constants of the macroelement are reported in Table 4. The comparison between experimental results and macroelement response for Rosquoët cyclic loading test is shown in Fig. 9.

3.2 Calibration using empirical equations

The procedure described in the previous Sect. 3.1 represents the "optimal" strategy for the calibration of the macroelement constants when some experimental data concerning the prototype response are available and a full 3d, non-linear finite element model of the soil-pile system can be used to run additional numerical tests (under monotonic conditions) to provide information on relevant aspects of the system response.

However, this procedure is both expensive from the experimental point of view and computationally quite demanding. Therefore it can be adopted only in cases where the importance of the project justifies the efforts. In this respect, it is interesting to explore the possibility that (at least) some of the macroelement constants could be deduced from empirical correlations deriving from decades of experience in the design of piled foundations in sandy soils. This is the main goal of this section.

As far as the failure locus of the macroelement is concerned, the constants H_0, M_0 and V_0 can be estimated using the formulas introduced by Meyerhof and his co-workers [49, 52]. In particular, the failure loads for pure horizontal loading, H_0, and pure bending, M_0, are given by [52]:

$$H_0 = 0.12\,\gamma d L_e^2 K_b \quad M_0 = 0.09\,\gamma d L_e^3 K_b \tag{30}$$

where γ is the soil unit weight; L_e the effective embedded length of the (flexible) pile, and K_b the net lateral pressure coefficient. The last two quantities are related to the empbedded pile length L, its relative bending stiffness and the soil peak friction angle by the following relations [48, 50]:

$$\frac{L_e}{L} = f_u \left(\frac{E_p I_p}{E_s d^4}\right)^{0.12} \qquad K_b = (1 - \sin\phi_p)\, N_q(\phi_p) \tag{31}$$

In Eq. (31), f_u is a dimensionless factor, equal to 1.65 for sand soils; E_s the average (secant) Young modulus of the soil along the pile lenght (assumed equal to 52.0 MPa); ϕ_p the sand peak friction angle (assumed equal to 39°), and N_q the bearing capacity factor proposed by Meyerhof [51], which for the given value of the peak friction angle is approximately equal to 110.

For a dry soil, the ultimate vertical bearing capacity of the pile in compression, V_{c0}, and in tension, V_{t0}, is given by [52]:

$$\begin{aligned} V_{c0} &= \left(\gamma L N_q\right) A_b + \left(\frac{1}{2}\gamma L\, K_s \tan\delta\right) A_s \\ V_{t0} &= \left(\frac{1}{2}\gamma L\, K_s \tan\delta\right) A_s \end{aligned} \tag{32}$$

where: $A_p = \pi d^2/4$ and $A_s = \pi d L$ are the pile base area and the lateral shaft surface, respectively; K_s is the average coefficient of earth pressure on the shaft, assumed equal to 0.5; and δ is the friction angle at the soil-pile interface, assumed equal to 27°.

It is worth noting that different values of H_0 can be calculated if the collapse mechanism for horizontal load is characterized by the formation of a plastic hinge along the pile shaft—see, e.g., Eurocode 7 [21]. However, since in Rosquoët tests the pile remained always elastic, this possibility has not been considered.

Table 3 Stiffness coefficients for a flexible pile embedded in sand provided by Eurocode 8–5 [22]

Soil model	$\frac{k_{hh}}{dE_{sd}}$	$\frac{k_{mm}}{dE_{sd}}$	$\frac{k_{hm}}{dE_{sd}}$ (*)
$E_s = E_{sd}\sqrt{\frac{z}{d}}$	$0.79\left(\frac{E_p}{E_{sd}}\right)^{0.28}$	$0.15\left(\frac{E_p}{E_{sd}}\right)^{0.77}$	$0.24\left(\frac{E_p}{E_{sd}}\right)^{0.53}$

(*) The sign of the coupling stiffness coefficient is opposite from the original value in Eurocode 8–5

The stiffness parameters k_{hh}, k_{mm} and k_{hm} can be evaluated using the formulas proposed by Gazetas [28] or those reported in Eurocode 8–5 [22], listed in Table 3. In the table, the soil profile considered is non-homogeneous, with the Young modulus of the soil E_s increasing with the square root of depth z. The reference value E_{sd} represents the value of E_s at $z = d$, and in this case has been assumed equal to 81 MPa. The vertical stiffness k_{vv} is evaluated from the finite element calculations presented in Sect. 3.1.

The values of the constants controlling the failure surface and the pseudo-elastic stiffness of the macroelement derived from Eqs. (30)–(32) and the formulas of Table 3 are summarized in Table 4. The empirical equations do not provide any information concerning the coupling coefficient α appearing in the expression of the failure surface, Eq. (14), or for the constants controlling the evolution of the internal displacement—and thus the macroelement behavior under cyclic loading. Therefore, the values obtained from the calibration procedure (a) have been retained for these quantities. In this respect, it is worth noting that the constant α—which controls the shape of the failure locus, not its size—is not likely to be affected by such system properties as pile length and diameter, soil strength and pile relative stiffness as the other failure-related constants $V_{\alpha 0}$, H_0 and M_0, and choosing a value α = 1.5 as a first approximation could be sufficiently accurate in most cases. Moreover, as discussed at the end of the previous Sect. 3.2, it is not difficult to estimate the constants controlling the cyclic behavior from the results of a cyclic horizontal loading test, a type of in-situ loading test which is relatively easy to perform and not too expensive. By comparing the results of the two calibration procedures shown in Table 4, it can be observed that the simplified Eqs. (30)–(32) may lead to a significant underestimation of V_{c0} and V_{t0} and, to a lesser extent, of M_0. This is due to the uncertainties related to the proper choice of the friction angle δ and the coefficient of earth pressure K_s at the pile-soil interface, and of the bearing capacity factor N_q, which reflects also on the computed value of M_0 via Eq. $(31)_2$. As for the pseudo-elastic stiffness coefficients, the main difference observed in the results of the two calibration procedures are in the large underestimation of the bending stiffness k_{mm} and of the coupling coefficient k_{hm} provided by the formulas of Table 3. Since the constant k_{hh} provided by the same source is slightly higher than the one obtained via 3d FE simulations, this limitation of Eurocode 8–5 formulas is likely to be due to the inadequacy of the linear elastic, inhomogeneous soil model for the particular problem at hand, rather than to the inappropriate choice of the reference modulus E_{sd}.

Table 4 Hypoplastic macroelement constants calibrated with the procedures (a) and (b) outlined in Sects. 3.1 and 3.2

Constant	Calibration (a) see Sect. 3.1	Calibration (b) see Sect. 3.2
H_0 (kN)	0.50×10^4	0.38×10^4
M_0 (kNm)	0.45×10^5	0.24×10^5
V_{c0} (kN)	2.50×10^4	0.96×10^4
V_{t0} (kN)	0.50×10^4	0.79×10^3
α (–)	1.50	
k_v (kN/m)	1.45×10^5	1.45×10^5
k_{hh} (kN/m)	2.39×10^5	2.58×10^5
k_{mm} (kN/m)	3.70×10^6	1.01×10^6
k_{hm} (kN/m)	8.03×10^5	3.75×10^5
κ (–)	1.2	
m_R (–)	5.0	
m_T (–)	2.0	
R (–)	6.0×10^{-3}	
β_r (–)	0.5	
χ (–)	0.5	

4 Macroelement validation

In the following, the predictive capabilities of the proposed macroelement for single piles in sand are assessed by comparing its predictions with the observed behavior for two additional cyclic horizontal loading tests from Rosquoët [64]—hereafter referred to as "Validation Test 1" and "Validation Test 2"—not previously used for the macroelement calibration. The two tests have been performed using the same small-scale pile model under artificial gravity, and the same foundation soil.

The two tests considered differ for the applied loading program: in Validation Test 1, a one-way horizontal cyclic horizontal load with $H_{\min}$ = 720 kN and $H_{\max}$ = 960 kN has been applied; in Validation Test 2, a fully symmetric, two-way horizontal cyclic load has been imposed, with $H_{\max} = -H_{\min}$ = 960 kN, see [64] for details.

In the macroelement simulations, both sets of model constants reported in Table 4 have been adopted, to assess the level of accuracy which can be achieved using both "optimal" and "approximate" calibration procedures.

4.1 Macroelement performance with calibration procedure (a)

The comparison between the experimentally observed response of the pile-soil system and the macroelement performance—when calibration procedure (a) is adopted—is shown in Fig. 10 for Validation Test 1, and in Fig. 11 for Validation Test 2. From the results shown in both figures it is apparent that the macroelement is capable of reproducing quite well the observed response of the pile-soil system for both one and two-way cyclic loading conditions. In particular, the coupling between horizontal and bending responses is correctly captured under monotonic loading conditions. The only significant difference between test results and model predictions is in the underestimation of accumulated permanent rotations in Validation Test 1 (see Fig. 10c). This is a consequence of the simplifying hypothesis of "associative" behavior of the macroelement, and could be corrected by using a slightly different potential function in place of f in Eq. (22).

4.2 Macroelement performance with calibration procedure (b)

The comparison between the experimentally observed response of the pile-soil system and the macroelement performance—when calibration procedure (b) is adopted—is shown in Fig. 12 for Validation Test 1, and in Fig. 13 for Validation Test 2. In this case, the objective of the comparison is to assess the impact of the simplified calibration procedure on the quality of the predictions.

The substantially good performance shown by the macroelement for both Validation Tests clearly indicate that—in this case—the underestimation of the vertical and bending collapse loads, V_{c0} and M_0, has only a minor impact on the quality of the macroelement predictions. The only relevant discrepancy between predictions and measurements found in this second series of simulations refers to the overestimation of the pile head rotations associated to its horizontal displacements (Figs. 12c, 13c). As the phenomenon is apparent in both the monotonic and the cyclic stages of the simulations, its cause is to be attributed mainly to the underestimation of the coupling stiffness coefficient k_{hm} provided by the Eurocode 8–5 formulas.

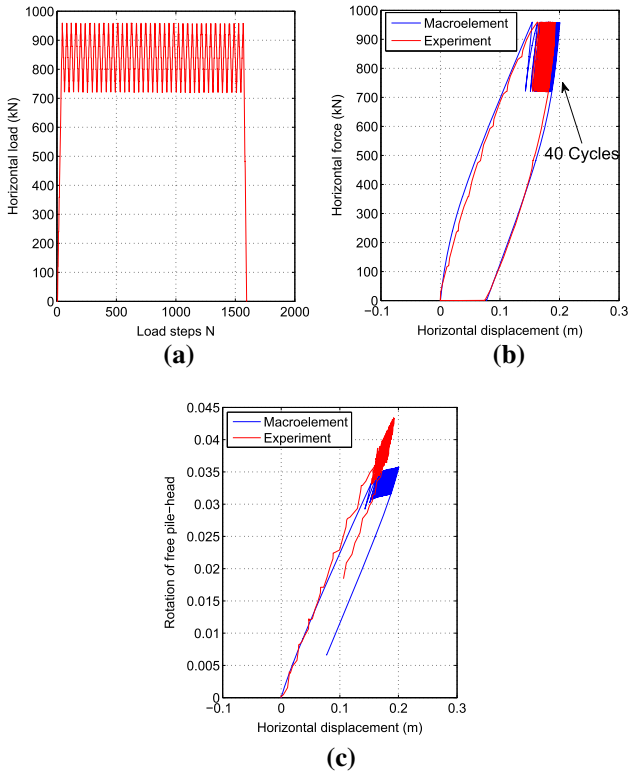

Fig. 10 Validation Test 1 with one-way loading: macroelement predictions using model constants from calibration procedure (**a**) and experimental results after [64]. **a** horizontal load versus number of steps; **b** horizontal force versus horizontal displacement at pile head; **c** rotation versus horizontal displacement at pile head

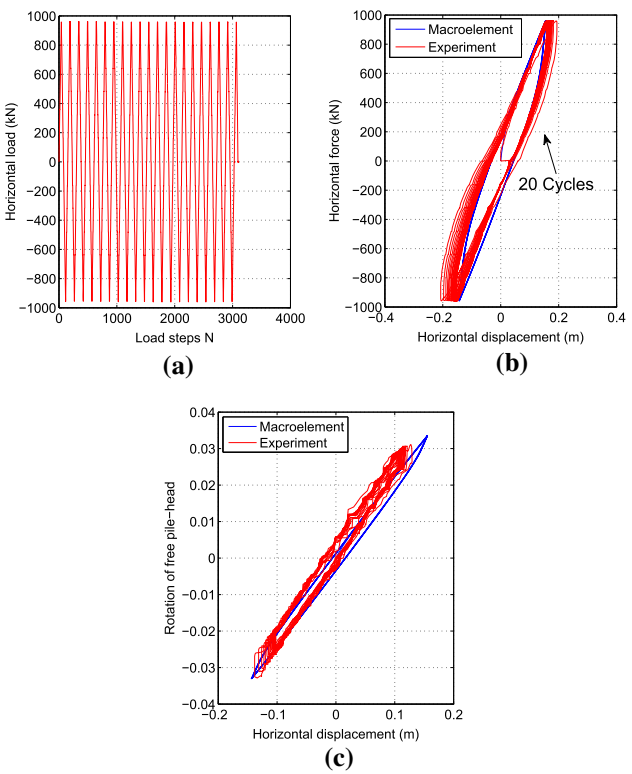

Fig. 11 Validation Test 2 with two-way loading: macroelement predictions using model constants from calibration procedure (**a**) and experimental results after [64]. **a** horizontal load vs. number of steps; **b** horizontal force versus horizontal displacement at pile head; **c** rotation versus horizontal displacement at pile head

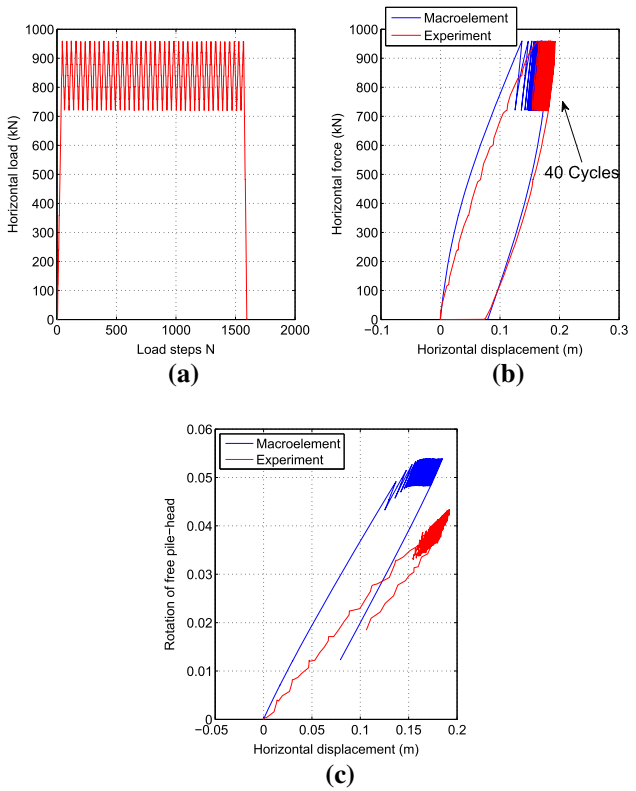

Fig. 12 Validation Test 1 with one-way loading: macroelement predictions using model constants from calibration procedure (**b**) and experimental results after [64]. **a** horizontal load versus number of steps; **b** horizontal force versus horizontal displacement at pile head; **c** rotation versus horizontal displacement at pile head

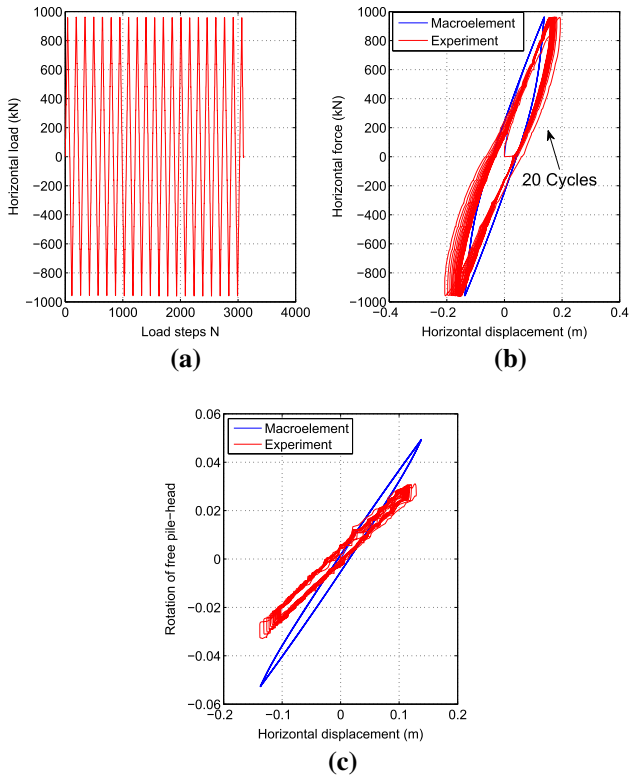

Fig. 13 Validation Test 2 with two-way loading: macroelement predictions using model constants from calibration procedure (**b**) and experimental results after [64]. **a** horizontal load versus number of steps; **b** horizontal force versus horizontal displacement at pile head; **c** rotation versus horizontal displacement at pile head

In spite of this limitation, the results of the validation exercise for the macroelement calibrated with the simplified procedures outlined in Sect. 3.2 can be considered quite satisfactory, in view of the potential application of the model in full SFSI analyses aimed at performance-based design of engineering structures.

5 Applicability to piles in layered soil profiles

Strictly speaking, the proposed hypoplastic macroelement is formulated for a single pile embedded in a homogeneous soil layer. However, some studies [29, 31] show that in piles subject to lateral loading, only a relatively small upper portion of the pile—called "active length"—significantly affects the pile response. For example, Gazetas and Dobry [29] point out that piles do not deform over their entire length: below the active length deflections, shear loads and bending moments become negligible.

Based on these observations, it might be tempting to extend the range of applicability of the proposed macroelement formulation to single piles in layered soils, provided that the applied loading at the pile head is mainly composed by a horizontal load increment and/or a bending moment increment, and that the soil profile is homogeneous within the entire active length of the pile.

To explore this possibility, an additional series of parametric FE simulations have been carried out with the FE model shown in Figure 14, to identify the active length for the problem examined in Sects. 3 and 4. In this model, a single pile identical to the one considered in previous Sects. 3 and 4 is embedded in a two-layer soil mass. The upper layer—modeled with the von Wolffersdorff hypoplastic model—has the properties of Fountainebleau sand. The lower layer is considered as isotropic and linear elastic, and is characterized by a Young's modulus E_{s2} = 280.0 MPa, and a Poisson's ratio ν_{s2} = 0.25.

In the parametric study, different monotonic horizontal load tests have been carried out considering different ratios $\eta = H_1/H \in [0, 1]$, where H is the depth to the bottom rigid boundary, and H_1 is the thickness of the upper hypoplastic layer. The horizontal load versus horizontal deflection curves obtained for different values of η are shown in Fig. 15. From the results reported in the figure, it is clear that the pile-soil response is unaffected by a non-

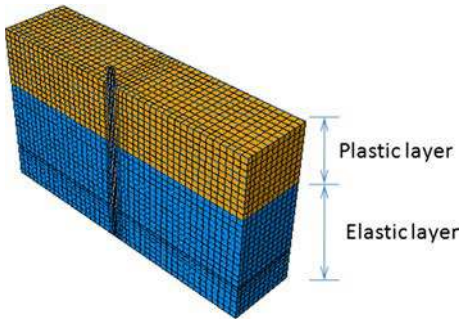

Fig. 14 FE model adopted for the identification of the active length of the pile

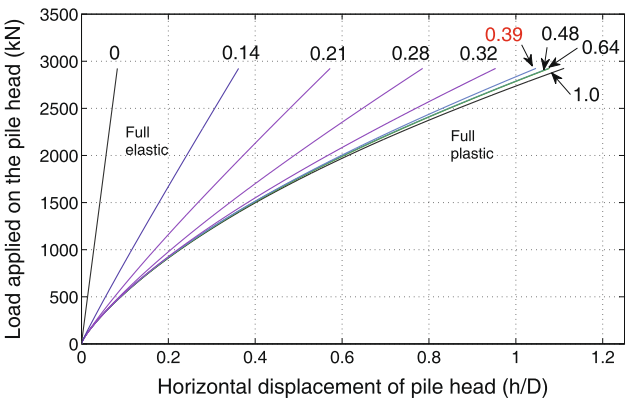

Fig. 15 Horizontal load versus horizontal displacement curves for different values of the thickness ratio η

homogeneous soil profile if, for the case at hand, η is equal or larger than 0.39. This figure corresponds to a thickness of the upper layer of 6.53 m, that is, to an active length of about 50 % of the pile length L.

A situation in which the soil can be considered as homogeneous for at least the upper 50 % of the pile length is not unusual in end-bearing piles, where the pile is driven (or bored) for a significant part of its length through soft, often quite homogeneous, soils to reach a deeper, much stronger and stiffer layer.

6 Conclusions

In this paper a novel hypoplastic macroelement for single vertical piles in sand has been presented, with the objective of providing a simple, efficient and yet accurate tool for the modeling of complex SFSI problems characterized by cyclic/dynamic loading conditions. Inspired by the work of Salciarini and Tamagnini for shallow foundations [68], the macroelement has been developed, in the generalized load/displacement setup, from the basic principles of the theory of hypoplasticity. In particular, the failure locus obtained by Li et al. [45] is a key ingredient in the formulation of the rate-type, incrementally non-linear constitutive equations. The introduction of a suitable displacement-like internal variable—the internal displacement—provides the model sufficient memory of past loading history to allow the modeling of the pile-soil system response for both monotonic and cyclic/dynamic loading conditions, although the failure surface might be slightly overpassed for specific loading conditions.

The important issue of the calibration of the constants defining the macroelement properties has been addressed in detail, presenting two possible calibration strategies. The first based on the combined use of experimental results from monotonic and cyclic loading tests, and advanced 3d FE simulations of monotonic loading conditions; the second exploiting the available knowledge of the failure and deformation behavior of single piles in sand to obtain most of the macroelement constants via simplified design formulas.

The excellent comparison between the macroelement predictions and the observed response in two different validation tests—with one-way and two-way cyclic loading programs—indicates that the proposed approach is capable of reproducing the pile-soil system behavior with the same level of accuracy of advanced non-linear 3d FE simulations, but with a dramatic reduction of the computational cost. This is particularly important for practical applications in which the foundation is subjected to a large number of cycles, such as, for example, performance-based earthquake design of structures or offshore enginering applications.

The relatively good performance shown by the macroelement even when calibrated using the simplified approach indicates that superior performance with respect to classical methods (like, for example, the BNWF approach) could be obtained without the need to consider expensive and relatively time-consuming calibration procedures. However, some attention has to be paid to the accurate characterization of the axial bearing capacity of the pile and of the "elastic" coupling stiffness coefficient k_{hm}.

Finally, the range of application of the proposed macroelement can be extended to piles in non-homogeneous soils if the pile is subjected mainly to horizontal load and/or bending moment increments at the pile head, and the soil is homogeneous within the active length of the pile. For the particular case considered in this study, a series of 3d FE results indicate that the active length of the pile is approximately 50 % of the embedded pile length.

Acknowledgments The financial support of IFSTTAR (Institut français des sciences et technologies des transports, de l'aménagement et des réseaux) and of the Région Pays de la Loire is gratefully

acknowledged. The authors would like also to thank the valuable support and help from the technical staff of the IFSTTAR centrifuge team. The first two authors would also like to thank the SINAPS@ project (Sésisme et Installation Nucléaire: Améliorer et Pérenniser la Sureté), approved and funded by the National Agency of Research (ANR) following the RSNR 2012 call for the projects on future investments post-Fukushima (SINAPS@ ANR-11-RSNR-0022). The fourth author acknowledges the financial support provided by the ReLUIS 2014–2016 Project, founded by the Italian Department of Civil Protection. The authors wish to thank the anonymous reviewers for their helpful and constructive comments, which greatly contributed to improving the final version of the paper.

References

1. Andria-Ntoanina I, Canou J, Dupla JC (2010) Caractérisation mécanique du sable de Fontainebleau NE34 à l'appareil triaxial sous cisaillement monotone. Tech. rep, Laboratoire Navier - Géotechnique (CERMES, ENPC/LCPC)
2. Banerjee P, Davies T (1978) The behaviour of axially and laterally loaded single piles embedded in nonhomogeneous soils. Géotechnique 28(3):309–326
3. Bartlett P (1976) Foundation rocking on clay soil. Department of Civil Engineering, University of Auckland
4. Boulanger RW, Curras CJ, Member S, Kutter BL, Wilson DW, Member A, Abghari A (1999) Seismic soil-pile-structure interaction experiments and analyses. J Geotech Geoenviron Eng 125(9):750–759. doi:10.1061/(ASCE)1090-0241(1999)125:9(750)
5. Budhu M, Davies TG (1987) Nonlinear analysis of laterality loaded piles in cohesionless soils. Can Geotech J 24(2):289–296
6. Calvetti F (2003) Limitations and perspectives of the micromechanical modelling of granular materials. Math Comput Model 37(5):485–495
7. Cambou B, Jean M, Radjai F (2013) Micromechanics of granular materials. Wiley, New York
8. Cassidy MJ, Byrne BW, Houlsby GT (2002) Modelling the behaviour of circular footings under combined loading on loose carbonate sand. Geotéchnique 52(10):705–712. doi:10.1680/geot.2002.52.10.705
9. Chatzigogos C, Pecker A, Salençon J (2009) Macroelement modeling of shallow foundations. Soil Dyn Earthq Eng 29(5):765–781. doi:10.1016/j.soildyn.2008.08.009
10. Correia AA (2011) A Pile-Head Macro-Element Approach to Seismic Design of monoshaft-supported bridges. Ph.D., Università degli Studi di Pavia & Istituto Universitario di Studi Superiori
11. Crémer C, Pecker A, Davenne L (2001) Cyclic macro-element for soil-structure interaction: material and geometrical non-linearities. Int J Numer Anal Meth Geomech 25(13):1257–1284. doi:10.1002/nag.175
12. Crémer C, Pecker A, Davenne L (2002) Modelling of nonlinear dynamic behaviour of a shallow strip foundation with macro-element. J Earthq Eng 6(2):175–211. doi:10.1080/13632460209350414
13. Cundall PA, Strack ODL (1979) A discrete numerical model for granular assemblies. Géotechnique 29(1):47–65. doi:10.1680/geot.1979.29.1.47
14. Curras C, Boulanger R, Kutter B, Wilson D (2001) Dynamic experiments and analyses of a pile-group-supported structure. J Geotech Geoenviron Eng 127(7):585–596. doi:10.1061/(ASCE)1090-0241(2001)127:7(585)
15. Darve F (1978) Une formulation incrémentale des lois rhéologiques. Application aux sols. Ph.D., INP Grenoble
16. Darve F (2002) Geomaterials: constitutive equations and modelling. CRC Press, Boca Raton
17. Davenne L, Brenet C (1998) Macro-éléments de poutres en béton armé. Tech. rep., LMT Cachan, num. 210, juin
18. Davies TG, Budhu M (1986) Non-linear analysis of laterally loaded piles in heavily overconsolidated clays. Géotechnique 36(4):527–538. doi:10.1680/geot.1986.36.4.527
19. El Shamy U (2008) DEM Simulation of the seismic response of shallow foundation on liquefiable soil. In: Geotechnical Earthquake Engineering and Soil Dynamics IV, pp. 1–10. American Society of Civil Engineers, Reston, VA. doi:10.1061/40975(318)119
20. Elachachi S (1992) Sur l'élaboration d'une méthode simplifiée d'analyse des structures de Génie Civil par macro-éléments adaptés aux constructions composites et endommageables. Ph.D., Université Paris VI
21. Eurocode7 (2003) Eurocode7: Geotechnical design. European Committee for Standardization (CEN), Belgium
22. Eurocode8-Part5 (2003) Eurocode 8: Design of structures for earthquake resistance - Part 5: Foundations, retaining structures and geotechnical aspects. European Committee for Standardization (CEN), Belgium
23. Figini R, Paolucci R, Chatzigogos CT (2012) A macro-element model for non-linear soil- shallow foundation-structure interaction under seismic loads : theoretical development and experimental validation on large scale tests. Earthq Eng Struct Dyn 41(3):475–493. doi:10.1002/eqe
24. Filippou F, Constandines M (2004) FedeasLab getting started guide and simulations examples. Ph.D. thesis, University of California, Berkeley, CA
25. Gajan S (2006) Physical and numerical modeling of nonlinear cyclic load-deformation behavior of shallow foundations supporting rocking shear walls, Ph.D., University of California, Davis
26. Gajan S, Raychowdhury P, Hutchinson TC, Kutter BL, Stewart JP (2010) Application and validation of practical tools for nonlinear soil-foundation interaction analysis. Earthq Spectra 26(1):111–129
27. Gajan S, Kutter BL (2009) Contact interface model for shallow foundations subjected to combined cyclic loading. J Geotech Geoenviron Eng 135(3):407–419
28. Gazetas G (1991) Foundation vibrations. In: Fang HY (ed) Foundation engineering handbook. Springer, US, pp 553–593. doi:10.1007/978-1-4615-3928-5_15
29. Gazetas BG, Dobry R (1984) Horizontal response of piles in layered soils. J Geotech Eng 110(1):20–40. doi:10.1061/(ASCE)0733-9410(1984)110:1(20)
30. Gerolymos N, Gazetas G (2006) Development of Winkler model for static and dynamic response of caisson foundations with soil and interface nonlinearities. Soil Dyn Earthq Eng 26(5):363–376. doi:10.1016/j.soildyn.2005.12.002
31. Gerolymos N, Gazetas G (2006) Static and dynamic response of massive caisson foundations with soil and interface nonlinearities-validation and results. Soil Dyn Earthq Eng 26(5):377–394. doi:10.1016/j.soildyn.2005.12.001
32. Gerolymos N, Gazetas G (2006) Winkler model for lateral response of rigid caisson foundations in linear soil. Soil Dyn Earthq Eng 26(5):347–361. doi:10.1016/j.soildyn.2005.12.003
33. Gottardi G, Houlsby G, Butterfield R (1999) Plastic response of circular footings on sand under general planar loading. Géotechnique 49(4):453–469
34. Grange S, Kotronis P, Mazars J (2009) A macro-element to simulate 3D soil-structure interaction considering plasticity and uplift. Int J Solids Struct 46(20):3651–3663. doi:10.1016/j.ijsolstr.2009.06.015

35. Grange S, Kotronis P, Mazars J (2009) A macro-element to simulate dynamic soil–structure interaction. Eng Struct 31(12):3034–3046. doi:10.1016/j.engstruct.2009.08.007
36. Grange S, Botrugno L, Kotronis P, Tamagnini C (2010) The effects of ioil-itructure interaction on a reinforced concrete viaduct. Earthq Eng Struct Dyn 40(1):93–105. doi:10.1002/eqe
37. Gudehus G, Amorosi A, Gens A, Herle I, Kolymbas D, Masín D, Muir Wood D, Niemunis A, Nova R, Pastor M, Tamagnini C, Viggiani G (2008) The soilmodels.info project. Int J Numer Anal Meth Geomech 32(12):1571–1572. doi:10.1002/nag.675
38. Harden CW, Hutchinson TC (2009) Beam-on-nonlinear-winkler-foundation modeling of shallow, rocking-dominated footings. Earthq Spectra 25(2):277–300
39. Hardin B, Drnevich V, Wang J, Sams C (1994) Resonant column testing at pressures up to 3.5 MPa (500 psi). Dyn Geotech Test II ASTM STP 1:222–233
40. Kolymbas D (1991) An outline of hypoplasticity. Arch Appl Mech 61(3):143–151
41. Kotronis P, Mazars J (2005) Simplified modelling strategies to simulate the dynamic behaviour of R/C walls. J Earthq Eng 9(2):285–306. doi:10.1080/13632460509350543
42. Le Pape Y, Sieffert JG (2001) Application of thermodynamics to the global modelling of shallow foundations on frictional material. Int J Numer Anal Meth Geomech 25(14):1377–1408. doi:10.1002/nag.186
43. Lewis RW, Schrefler BA (1987) The finite element method in the deformation and consolidation of porous media. Wiley, New York
44. Li Z (2013) Etude experimentale et numerique de fondations profondes sous sollicitations sismiques: pieux verticaux et pieux inclines - experimental and numerical study of deep foundations under seismic loading: vertical piles and inclined piles. Ph.D., Ecole Centrale de Nantes https://hal.archives-ouvertes.fr/tel-01095508. (in English)
45. Li Z, Kotronis P, Escoffier S (2014) Numerical study of the 3D failure envelope of a single pile in sand. Comput Geotech 62:11–26. doi:10.1016/j.compgeo.2014.06.004
46. Martin CM, Houlsby GT (2001) Combined loading of spudcan foundations on clay: numerical modelling. Géotechnique 51(8):687–699. doi:10.1680/geot.2001.51.8.687
47. Mazars J, Kotronis P, Ragueneau F, Casaux G (2006) Using multifiber beams to account for shear and torsion. Comput Methods Appl Mech Eng 195(52):7264–7281. doi:10.1016/j.cma.2005.05.053
48. Meyerhof GG (1951) The ultimate bearing capacity of foudations. Geotéchnique 2(4):301–332. doi:10.1680/geot.1951.2.4.301
49. Meyerhof BGG, Yalcin S, Mathur SK (1983) Ultimate pile capacity for eccentric inclined load. J Geotech Eng 109(3):408–423. doi:10.1061/(ASCE)0733-9410(1983)109:3(408)
50. Meyerhof GG, Sastry VVRN, Yalcin AS (1988) Lateral resistance and deflection of flexible piles. Can Geotech J 25(3):511–522. doi:10.1139/t88-056
51. Meyerhof GG (1995) Behaviour of pile foundations under special loading conditions 1994 R.M. Hardy keynote address. Can Geotech J 32(2):204–222. doi:10.1139/t95-024
52. Meyerhof GG, Ghosh DP (1989) Ultimate capacity of flexible piles under eccentric and inclined loads. Can Geotech J 26(1):34–42. doi:10.1139/t89-004
53. Montrasio L, Nova R (1997) Settlements of shallow foundations on sand: geometrical effects. Geotéchnique 47(1):49–60
54. Murchison JM, O'Neill MW (1984) Evaluation of p-y relationships in cohesionless soils. In: Analysis and design of pile foundations, pp. 174–191. ASCE
55. Niemunis A (2002) Extended hypoplastic models for soils. Thesis, Bochum University
56. Niemunis A, Herle I (1997) Hypoplastic model for cohesionless soils with elastic strain range. Mech Cohes Frict Mater 2:279–299
57. Nogami T, Otani J, Konagai K, Chen H (1992) Nonlinear soil-pile interaction model for dynamic lateral motion. J Geotech Eng 118(1):89–106. doi:10.1061/(ASCE)0733-9410(1992)118:1(89)
58. Nova R, Montrasio L (1991) Settlements of shallow foundations on sand. Geotéchnique 41(2):243–256. doi:10.1680/geot.1991.41.2.243
59. Paolucci R (1997) Simplified evaluation of earthquake-induced permanent displacements of shallow foundations. J Earthq Eng 1(3):563–579. doi:10.1080/13632469708962378
60. Pastor M, Tamagnini C (2004) Numerical modelling in geomechanics. Kogan Page Limited, London
61. Pender M, Wotherspoon L, Sa'don NM, Orense R (2012) Macro element for pile head cyclic lateral loading. In: Sakr MA, Ansal A (eds) Special topics in earthquake geotechnical engineering, geotechnical, geological and earthquake engineering, vol 16. Springer, Dordrecht, pp 129–145. doi:10.1007/978-94-007-2060-2
62. Pham BH, Brancherie D, Davenne L, Ibrahimbegovic A (2012) Stress-resultant models for ultimate load design of reinforced concrete frames and multi-scale parameter estimates. Comput Mech 51(3):347–360. doi:10.1007/s00466-012-0734-6
63. Rha C, Taciroglu E (2007) Coupled macroelement model of soil–structure interaction. J Eng Mech 133(12):1326–1340. doi:10.1061/(ASCE)0733-9399(2007)133:12(1326)
64. Rosquoët F (2004) Pile under lateral cyclic load. Ph.D., Ecole Centrale & Université de Nantes
65. Salciarini D, Tamagnini C, Grange S, Kotronis P (2010) La modellazione dei fenomeni di interazione terreno struttura mediante macroelementi: elastoplasticità vs. ipoplasticità. Rivista Italiana di Geotecnica 4(2010):9–28
66. Salciarini D, Bienen B, Tamagnini C (2014) Incorporating scale effects in shallow footings in a hypoplastic macroelement model. Numer Methods Geotech Eng 1:397
67. Salciarini D, Bienen B, Tamagnini C (2011) A hypoplastic macroelement for shallow foundations subject to six-dimensional loading paths. In: Proceedings international symposium on computational geomechanics (ComGeo II), Cavtat-Dubrovnik, Croatia
68. Salciarini D, Tamagnini C (2009) A hypoplastic macroelement model for shallow foundations under monotonic and cyclic loads. Acta Geotech 4(3):163–176. doi:10.1007/s11440-009-0087-2
69. Scott MH, Fenves GL (2006) Plastic hinge integration methods for force-based beamcolumn elements. J Struct Eng 132(2):244–252. doi:10.1061/(ASCE)0733-9445(2006)132:2(244)
70. Shirato M, Paolucci R, Kouno T, Nakatani S, Fukui J, Nova R, di Prisco C (2009) Numerical simulation of model tests of pier-shallow foundation systems subjected to earthquake loads using an elasto-uplift-plastic macro element. Soils Found 48(5):693–711
71. Šmilauer V, Catalano E, Chareyre B, Dorofenko S, Duriez J, Gladky A, Kozicki J, Modenese C, Scholtès L, Sibille L, Stránskỳ J, Thoeni K (2010) Yade Documentation, first edn. The Yade Project http://yade-dem.org
72. Storie L, Pender M, Clifton G, Wotherspoon L (2014) Soil-foundation-structure interaction for buildings on shallow foundations in the christchurch earthquake. In Proceedings 10NCEE, Anchorage, Alaska
73. Taciroglu E, Rha C, Wallace JW (2006) A robust macroelement model for soil-pile interaction under cyclic loads. J Geotech Geoenviron Eng 132(10):1304–1314. doi:10.1061/(ASCE)1090-0241(2006)132:10(1304)

74. Tamagnini C, Salciarini D, Ragni R (2013) Implementation of 6–dof hypoplastic macroelement in a finite element code. In: Proceedings of third international symposium on computational geomechanics (ComGeo III). Berlin: Springer
75. Tamagnini C, Viggiani G (2002) Constitutive modelling for rate-independent soils: a review. Revue française de génie civil 6(6):933–974
76. Tamagnini C, Viggiani G, Chambon R (2000) A review of two different approaches to hypoplasticity. In: In constitutive modelling of granular materials, pp. 107–145. Springer Berlin
77. Varun (2010) A non-linear dynamic macroelement for soil structure interaction analysis of piles in liquefiable sites. Ph.D., Georgia Institute of Technology
78. von Wolffersdorff PA (1996) A hypoplastic relation for granular materials with a predefined limit state surface. Mechanics of Cohesive-Frictional Materials 1(4):251–271. doi:10.1002/(SICI)1099-1484(199607)1:3<251:AID-CFM13>3.0.CO;2-3
79. Wiessing P (1979) Foundation rocking on sand. Department of Civil Engineering, University of Auckland
80. Wotherspoon L, Pender J (2010) Effect of shallow foundation modeling on seismic response of moment frame structures. Soil–foundation–structure interaction. CRC Press, Taylor & Francis Group, New York, pp 117–124
81. Zienkiewicz OC, Chan A, Pastor M, Schrefler B, Shiomi T (1999) Computational geomechanics. Wiley, Chichester